2011 American Control Conference
on O'Farrell Street, San Francisco, CA, USA
June 29 - July 01, 2011

Modeling and Control Insights into Demand-side Energy Management through Setpoint Control of Thermostatic Loads

Saeid Bashash and Hosam K. Fathy*

Abstract— **This paper examines the problem of using thermostat offset signals to directly control distributed air conditioning loads attached to the grid. The paper models these loads using a novel partial differential equation framework that builds on existing diffusion-based load modeling ideas in the literature. Both this PDE model and its finite-difference discretizations are bilinear in the state and control variables. This key insight creates a unique opportunity for designing nonlinear direct load control algorithms with theoretically guaranteed Lyapunov stability properties. The paper's main contribution to the literature is the development of the bilinear PDE model and Lyapunov-stable controller for real-time management of thermostatic air conditioning loads.**

I. Introduction

This paper studies the problem of controlling the aggregate load imposed on the power grid by thermostatic air conditioning systems. We develop a novel partial differential equation framework for modeling these systems' temperature distributions. Furthermore, we design a Lyapunov-stable algorithm that assumes these systems' aggregate load to be measurable, and broadcasts a global thermostatic offset signal to control it.

In a broad sense, this paper examines demand-side energy management, defined as the process through which a smart grid can adjust the power demands of the loads it serves. The importance of demand-side energy management is increasing as: *(i)* the nation's need for electricity grows, and *(ii)* intermittent renewable resources are used to meet more of this need [1,2]. Researchers have identified different types of candidate loads for demand-side energy management, including air conditioners [2-4], water heaters [5,6], plug-in electric vehicles [7,8], etc. One can manage these loads through economic means (e.g., real-time pricing) or direct load control, the focus of this paper. The overarching goal of this paper is to develop stable direct load control algorithms specifically for air conditioning loads. We assume these air conditioning loads to be thermostatically controlled, and seek a control algorithm that adjusts their aggregate power demand by broadcasting a small global offset to their thermostat setpoints. This is a challenging problem due to the complex aggregated dynamics of these thermostatic air conditioning loads. We therefore seek a modeling and control framework that makes it possible to control these loads in a Lyapunov-stable manner despite this complexity.

The existing literature on aggregated air conditioning load modeling was originally motivated by the "cold load pickup" problem [9]. Cold load pickup can be induced when, for instance, a utility responds to peak grid demand by temporarily shedding the air conditioning loads of consenting clients. Upon restoration of power to these clients, their air conditioners typically demand full power in unison, resulting in a new "cold load pickup" peak. The literature presents a variety of models for predicting both cold load pickup and other aggregate air conditioning system dynamics. These include regression models based on past data [10], physics-based models [11], and stochastic Fokker-Planck diffusion models [12]. This paper builds on a recent study by Callaway that uses a Fokker-Planck model to study the effectiveness of utilizing setpoint temperature offset signals to control the aggregate demands of thermostatic air conditioning loads [2]. Callaway linearized this model for small perturbations around nominal operating conditions, and developed a viable direct load control algorithm based on this linearization. Our work is similar to Callaway's excellent research in one respect: we show that for slow setpoint temperature variations, aggregate load dynamics are accurately modeled using two coupled partial differential equations. These PDEs represent the diffusion of different air conditioning loads' temperatures within the deadbands of their thermostats. A key insight, highlighted in this paper for the first time, is the fact that both these diffusion PDEs and their finite-difference discretizations are bilinear in terms of aggregate state and control input variables. This insight motivates this paper's most important original contribution to the literature, namely, the development of Lyapunov-stable algorithms for direct air conditioning load control. The current version of this paper develops one type of Lyapunov-stable control methods that require both state and output feedback. Parallel to this effort, we are also investigating a sliding mode robust control design that can achieve Lyapunov stability without requiring full-state feedback.

The remainder of the paper is organized as follows. Section II presents a physics-based model of a single thermostatically controlled load (TCL), then aggregates this model using a Monte Carlo method. Section III then derives

S. Bashash is with the Department of Mechanical Engineering, the University of Michigan, Ann Arbor, MI 48109.

H. K. Fathy is with the Department of Mechanical Engineering, Pennsylvania State University, University Park, PA 16802.

*Address all correspondence to this author, hkf2@psu.edu.

a control-oriented, PDE-based model of the aggregate load, and Section IV validates this PDE model vis-à-vis the Monte Carlo "primary model". Section V designs the Lyapunov-stable direct load controller for the PDE model, and demonstrates its performance in simulation. Finally, Section VI summarizes the paper's key contributions.

II. PRIMARY TCL MODEL

This section introduces a physics-based model of a single thermostatically controlled load, then uses Monte Carlo simulation to simulate the aggregate dynamics of many TCLs. We will refer to the resulting aggregate TCL dynamics model as the "primary model". Section III will then use continuum approximations to create a PDE-based representation of these aggregate dynamics. This PDE representation will make it possible to design Lyapunov-stable controllers for aggregate TCL dynamics.

A. Primary model for aggregate TCLs

Consider a large family of thermostatically controlled loads. Suppose that the internal and ambient temperatures corresponding to each load, i, are T_i and $T_{\infty,i}$, respectively (in ^{o}C). Suppose, furthermore, that this load can be modeled as a thermal capacitance, C_i (kWh/^{o}C), in series with a thermal resistance, R_i (^{o}C/kW). Finally, let the binary variable $s_i(t)$ denote whether the load's air conditioner is on or off, and let the rate at which the air conditioner absorbs (or injects) heat from the load when turned on be P_i (kW). Then, one can model the dynamics of N_L loads using a set of independent first-order ordinary differential equations [2]:

$$\dot{T}_i(t) = \frac{1}{C_i R_i}\left(T_{\infty,i} - T_i(t) - s_i(t) R_i P_i\right), \quad i = 1, 2, ..., N_L \tag{1}$$

Supposing that the on/off signal $s_i(t)$ is governed by a thermostatic switching law with some deadband, i.e.,

$$s_i(t) = \begin{cases} 0 & \text{if } \; s_i(t-\varepsilon_t) = 1 \;\; \& \;\; T_i(t) \le T_{\min,i} \\ 1 & \text{if } \; s_i(t-\varepsilon_t) = 0 \;\; \& \;\; T_i(t) \ge T_{\max,i} \\ s_i(t-\varepsilon_t) \end{cases} \tag{2}$$

where $T_{\max,i}$ and $T_{\min,i}$ are the upper and the lower limits of temperature deadband, and ε_t is the simulation time step.

Now suppose that the upper and lower extremes of the above deadband are related to some setpoint temperature, $T_{sp,i}$,, as follows:

$$T_{\min,i} = T_{sp,i} - \frac{\Delta_{db,i}}{2}; \;\; T_{\max,i} = T_{sp,i} + \frac{\Delta_{db,i}}{2} \tag{3}$$

where Δ_{db} is the width of the temperature deadband, which should be made small in order for the temperature to stay around the desired set-point.

The aggregate TCL load can now be obtained as:

$$P_T(t) = \sum_{i=1}^{N_L} \frac{1}{\eta_i} P_i s_i(t) \tag{4}$$

where η_i is the power system's transmission efficiency.

The overarching goal of this paper is to achieve demand-side management of the above TCLs, meaning: to control their aggregate load , $P_T(t)$. One way to achieve this is to broadcast a universal control signal that offsets the individual loads' setpoint temperatures as follows:

$$T_{sp,i}(t) = T_{sp0,i} + \lambda_i f(t); \;\; -1 \le f(t) \le 1 \tag{5}$$

In Eq. (5), $T_{sp0,i}$ is the initial set-point temperature, $f(t)$ is the dimensionless universal control signal sent to all of the individual loads, and the parameter λ_i represents each load's receptiveness to the control command. Larger values of the parameter λ_i provide greater control authority over aggregate load, at the expense of possibly greater setpoint temperature variations, and vice versa. In practice, the value of this parameter can depend on the type of load at hand. For air conditioning systems, for instance, one may choose λ conservatively (e.g., in the order of Δ_{db}), whereas for water heaters it may be reasonable to adopt larger values.

B. Numerical simulations

This section presents two simulation studies that highlight the effect of setpoint temperature variations on aggregate load response. Both studies consider a population of 1,000 air conditioning systems. The first simulation study examines the free dynamics of aggregated TCLs with no external setpoint manipulation, whereas the second study examines their forced response. In examining the free response of TCLs, we consider both the case where their parameters are *homogeneous* and the case where the parameters are *heterogeneous*. In the homogeneous case, all TCLs have the parameter values listed in Table 1 (adopted from [2]). In the heterogeneous case, we distribute every parameter (i.e., C, P, R, Δ_{db} , η, T_{sp0}, and T_∞) normally around the nominal values in Table 1. The standard deviations of these independent parameter distributions are set to equal some fixed multiple of the corresponding mean values. In both the homogeneous and heterogeneous parameter cases, the initial distribution of TCL temperatures is set to the following non-steady-state condition: Two thirds of the loads are uniformly distributed along the temperature axis within the ON-state, and one third are uniformly distributed within the OFF-state.

Table 1. Parameter values for the numerical simulations (Taken from [2]).

Parameter	Value
R, Average thermal resistance	2^{o}C/kW
C, Average thermal capacitance	10 kWh/^{o}C
P, Average energy transfer rate	14 kW
η, Load efficiency	2.5
T_{sp0}, Initial set-point temperature	20^{o}C
T_∞, Ambient temperature	32^{o}C
Δ_{db}, Thermostat deadband	0.5^{o}C

Figure 1(a) depicts the aggregate power response to the above initial conditions. The plot includes the response of the homogeneous model, as well as the responses of three

heterogeneous models corresponding to different parameter standard deviation values (normalized with respect to each parameter's mean value). Examination of the plot shows that the homogeneous model exhibits oscillatory limit cycle behavior, while the heterogeneous models tend to damp these oscillations significantly over time. This damping effect increases with parameter heterogeneity. This relationship between parameter heterogeneity and damping, previously observed by Callaway [2], is extremely important because it makes aggregate TCL dynamics easier to control in a stable, non-oscillatory manner. Fortunately, there is some inherent degree of parameter heterogeneity in any practical aggregate TCL system.

Figure 1(b) depicts the temperature response of a few selected loads from the homogeneous model. The most interesting observation is perhaps the fact that the rates of temperature variation with time for each load appear nearly constant during both the cooling and heating phases. In reality, these rates are governed by the exponential solution to Equations (1-2), but for small temperature intervals such as the temperature deadband of the thermostat model here, they can be approximated by constant values.

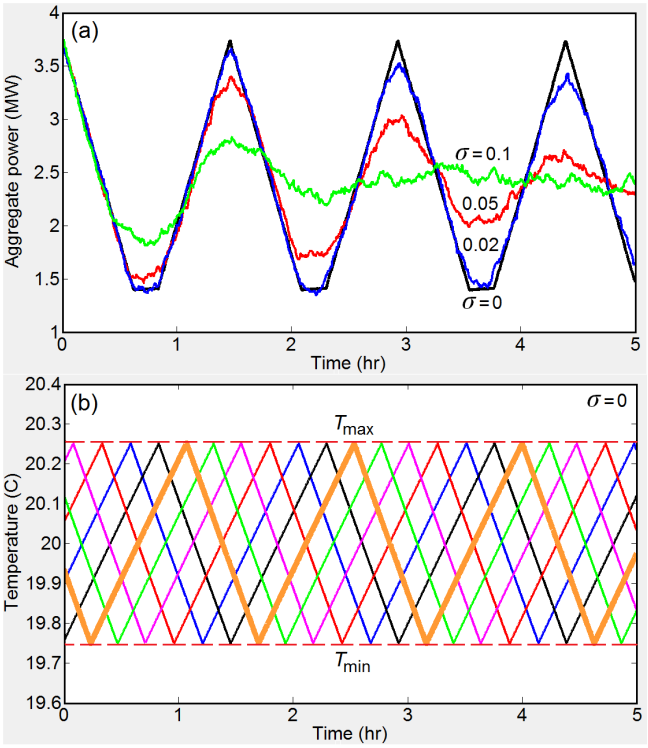

Fig. 1. Model simulation starting from a non-steady-state initial condition for a constant set-point temperature: (a) Aggregate power response for the homogenous model and the heterogeneous models with different standard deviation values, and (b) temperature responses of a few selected individual loads from the homogenous model.

In the second simulation, we vary the set-point temperature smoothly within a limited range and monitor the aggregate load response of the homogenous and the heterogeneous models. The set-point limits are set to $\lambda = \Delta_{db}/2$, that is, the set-point is allowed to vary within the initial deadband range. The same initial condition as the previous simulation is applied. Figure 2 depicts the applied set-point temperature and the resultant aggregated power trajectories for different parameter standard deviation values. The figure shows that even small variations in setpoint temperature provide significant control authority over aggregate TCL demand, thereby motivating the remainder of this work.

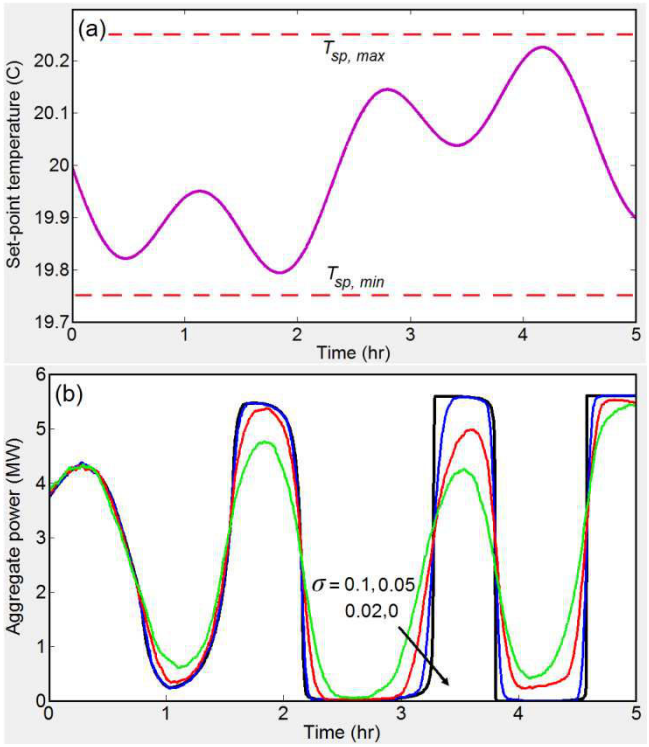

Fig. 2. (a) Set-point temperature variation, and (b) Aggregate power response for the homogenous model and the heterogeneous models with different standard deviation values

III. Development of a Control-Oriented Model for Aggregate TCLs

Controlling the aggregate air conditioning load represented by Equations (1-5) can be very challenging for at least two reasons. First, the model in Eq. (1-5) is hybrid, in the sense that it contains both continuously-varying state variables (i.e., temperatures) and discrete ON/OFF state variables (i.e., the thermostatic switching states). Second, the model represents each TCL using a separate set of state equations, and uses Monte Carlo simulation to account for heterogeneity in parameters and initial conditions. This implies that the model will have a very large order for any reasonable simulation study conditions.

To address the above two challenges, this section will use continuity approximations to aggregate Equations (1-5) into a pair of partial differential equations coupled at their boundaries. These partial differential equations will govern the diffusion of TCLs between the upper and lower bounds of their respective temperature deadbands. We will derive these PDEs for the free response of the TCLs first, then extend them to capture forced response dynamics and finally discretize them using finite differences. This derivation

extends earlier research by Callaway [2] and Melhame and Chong [12] by incorporating the setpoint offset signal directly as a control input in the coupled PDEs. It will assume parameter homogeneity among the TCLs, leaving the PDE-based modeling of heterogeneous loads as an open question for future research.

A. Development of a Continuum-Level Free Model

To develop a continuum-level free thermostatic load model, we assume that all the individual loads are distributed between the low-end and the high-end temperature limits. At any given time instant, some of the loads are in the ON-state, moving from the high-end temperature to the low-end temperature, while some others are in the OFF-state traveling in the opposite direction. The loads which hit the temperature boundaries change their thermostatic state from ON to OFF and vice versa. This migration of loads in opposite directions between the two temperature boundaries can be described by two separate linear diffusion processes with coupled boundaries, as discussed next.

Let X_{on} (T, t) and X_{off} (T, t) represent the distribution (concentration) of loads at time t and temperature T, respectively at the ON and OFF states. Then, assuming parameter homogeneity, the flux of the loads moving within the temperature bounds can be expressed as:

$$\begin{aligned} F_{on}(t,T) &= X_{on}(t,T)\frac{\delta T}{\delta t} \\ F_{off}(t,T) &= X_{off}(t,T)\frac{\delta T}{\delta t} \end{aligned} \tag{7}$$

where the term $\delta T/\delta t$ represents the variation of temperature with respect to time, which can be obtained from Eq. (1). The resultant fluxes (assuming that all the loads share the same parameter values) can then be recast as:

$$\begin{aligned} F_{on}(t,T) &= \frac{1}{CR}(T_\infty - T - RP)X_{on}(t,T) = \alpha_{on}(T_\infty,T)X_{on}(t,T) \\ F_{off}(t,T) &= \frac{1}{CR}(T_\infty - T)X_{off}(t,T) = \alpha_{off}(T_\infty,T)X_{off}(t,T) \end{aligned} \tag{8}$$

where α_{on} and α_{off} represent the local diffusion rates of the loads. For a constant ambient temperature, and neglecting the variation of temperature around the initial setpoint temperature, these parameters can be approximated by their constant average values as:

$$\begin{aligned} \alpha_{on}(T_\infty,T) &\cong \bar{\alpha}_{on}(T_\infty,T_{sp0}) = \frac{1}{CR}(T_\infty - T_{sp0} - RP) \\ \alpha_{off}(T_\infty,T) &\cong \bar{\alpha}_{off}(T_\infty,T_{sp0}) = \frac{1}{CR}(T_\infty - T_{sp0}) \end{aligned} \tag{9}$$

These values respectively correspond to the average slope of the falling and rising temperature trajectories of the individual loads as shown in Figure (1). In the remaining derivations, we will use the exact expressions for α_{on} and α_{off}. However, their average values will be used for numerical simulations.

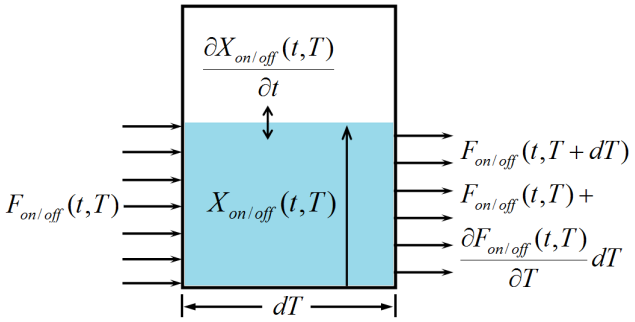

Fig. 3. A small control volume with entering and exiting fluxes, and their relation to the variation of load concentration inside the control volume.

For a small control volume of length dT, the rate of increase of the load concentration is given by the difference between the entering flux and the exiting flux divided by the length of the control volume (see Figure 3):

$$\begin{aligned} \frac{\partial X_{on/off}(t,T)}{\partial t} &= \frac{1}{dT}\left\{F_{on/off}(t,T) - F_{on/off}(t,T+dT)\right\} \\ &= -\frac{\partial F_{on/off}(t,T)}{\partial T} \end{aligned} \tag{10}$$

Merging Eq. (8) into Eq. (10), we can obtain the governing partial differential equation (PDE) of the system:

$$\frac{\partial X_{on/off}(t,T)}{\partial t} = -\frac{\partial\left[\alpha_{on/off}X_{on/off}(t,T)\right]}{\partial T} \tag{11}$$

This equation represents two first-order linear diffusion processes, yet, we need to define the boundary conditions. Since the loads crossing the boundaries change their ON/OFF state, the loads that exit the OFF state will enter the ON state at the high-end boundary, and the loads that exit the ON state will enter the OFF state at the low-end boundary. This interchange of loads at the boundaries is equivalent to equating the entering and the exiting fluxes at the boundaries, which can be expressed as:

$$\left[\alpha_{on}(T_\infty,T)X_{on}(t,T)\right]_{@\,T=\substack{T_{\min}\\T_{\max}}} = -\left[\alpha_{off}(T_\infty,T)X_{off}(t,T)\right]_{@\,T=\substack{T_{\min}\\T_{\max}}} \tag{12}$$

The total aggregated power can be obtained by integrating the distribution of loads at the ON-state over the specified temperature range and multiplying it by the net power consumed by each load:

$$P_T(t) = \frac{P}{\eta}\int_{T_{\min}}^{T_{\max}} X_{on}(t,\tau)d\tau \tag{13}$$

Equations (11)-(13) represent the continuum-level dynamics of the system with fixed set-point temperature. These equations are similar to the stochastic Fokker-Plank equations derived in [12], except that we have not included any disturbance term for simplicity.

In the next section, we develop a continuum level forced system model for TCLs to take into account the set-point temperature variation.

B. Development of a Continuum Level Forced Model

In the thermostatic load control scenario, the grid operator is able to vary the set-point temperature of the individual loads, altering their aggregate response. In such a forced system the temperature boundaries move with the set-point temperature. Thus, there will be different load exchange rates at the boundaries. Modeling the forced system is not straightforward in general. However, if we keep the rate of variation of the set-point temperature slower than the internal diffusion dynamics of the system, i.e., $\alpha_{on} < \dot{T}_{sp}(t) < \alpha_{off}$, there will be a simple way of incorporating the set-point temperature variation in the model. To do so, we assume the control volume shown in Figure (3) moves with the set-point temperature, as shown in Figure (4). The load flux experienced by the moving control volume can now be represented by the flux associated with a fixed control volume, obtained earlier, minus the flux introduced by the motion of the control volume:

$$\begin{aligned} F_{on}(t,T) &= X_{on}(t,T)\frac{\delta T}{\delta t} - X_{on}(t,T)\frac{dT_{sp}}{dt} \\ &= X_{on}(t,T)\left(\alpha_{on} - \dot{T}_{sp}(t)\right) \\ F_{off}(t,T) &= X_{off}(t,T)\frac{\delta T}{\delta t} - X_{off}(t,T)\frac{dT_{sp}}{dt} \\ &= X_{off}(t,T)\left(\alpha_{off} - \dot{T}_{sp}(t)\right) \end{aligned} \tag{14}$$

Following the same procedure carried out in the previous section, we obtain the following governing equations for the system with setpoint temperature variation:

$$\frac{\partial X_{on/off}(t,T)}{\partial t} = -\frac{\partial\left[\left(\alpha_{on/off} - \dot{T}_{sp}\right)X_{on/off}(t,T)\right]}{\partial T},\ \alpha_{on} < \dot{T}_{sp}(t) < \alpha_{off} \tag{15}$$

$$\left[\left(\alpha_{on} - \dot{T}_{sp}\right)X_{on}(t,T)\right]_{@\,T=\substack{T_{\min}\\T_{\max}}} = -\left[\left(\alpha_{off} - \dot{T}_{sp}\right)X_{off}(t,T)\right]_{@\,T=\substack{T_{\min}\\T_{\max}}} \tag{16}$$

Moving the setpoint temperature faster the load diffusion speed results in the separation of the loads from the temperature frame (i.e., the thermostatic deadband). Therefore, the above model will deviate from the actual system response in this scenario. Fortunately, in the problem outlined in this paper, the setpoint temperature is controlled by the grid operator, which can account for these constraints.

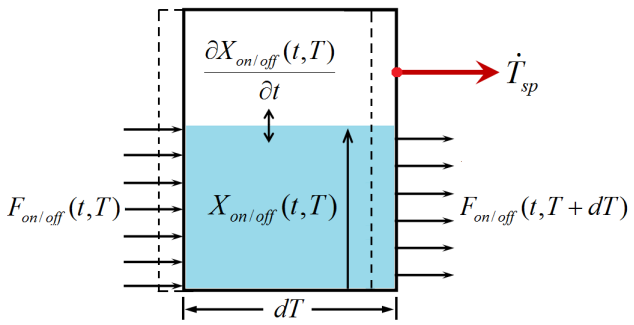

Fig. 4. A moving control volume for the forced model derivation.

Equations (15) and (16) represent the final continuum-level model of the forced system. In the next section, we discretize these equations using the finite-difference method to obtain a finite-dimensional state-space representation of the system for further analysis and controller design.

C. Finite-dimensional State-Space Model Development

In this section, we apply the method of finite differences to the derived model to obtain its state-space representation. This will provide a starting point for the control design. We discretize the temperature range between its two limits into small segments of uniform width. At each segment, there is a flux of TCLs entering the segment and a flux leaving it, both of which we will represent using the backward difference method. Figure 5 provides a schematic representation of this discretization. The resultant state-space equations after applying the backward difference method to Equation (15) and using the average values of the diffusion coefficients are given by:

$$\begin{aligned} \dot{x}_j(t) &= \frac{\bar{\alpha}_{off} - \dot{T}_{sp}}{\Delta T}\left(x_{j-1}(t) - x_j(t)\right), \quad j = 2,3,...,N \\ \dot{x}_j(t) &= \frac{\bar{\alpha}_{on} - \dot{T}_{sp}}{\Delta T}\left(-x_{j-1}(t) + x_j(t)\right), \quad j = N+2, N+3,...,2N \end{aligned} \tag{17}$$

where $x_j(t)$ denotes the number of loads at segment j, and $\Delta T = \Delta_{db}/N$ is the discretization length with N being the number of discrete segments in either the ON state or OFF state. The state-space equations given in (17) can be interpreted as follows: The rate of change of concentration of loads in a given temperature segment is equal to the flow of loads entering the segment, minus the flow of loads leaving it. Using the same interpretation, we can complete the state-space model derivation by obtaining the equations for the boundary segments, $x_1(t)$ and $x_{N+1}(t)$:

$$\begin{aligned} \dot{x}_1(t) &= -\frac{\bar{\alpha}_{off} - \dot{T}_{sp}}{\Delta T}x_1(t) - \frac{\bar{\alpha}_{on} - \dot{T}_{sp}}{\Delta T}x_{2N}(t) \\ \dot{x}_{N+1}(t) &= \frac{\bar{\alpha}_{off} - \dot{T}_{sp}}{\Delta T}x_N(t) + \frac{\bar{\alpha}_{on} - \dot{T}_{sp}}{\Delta T}x_{N+1}(t) \end{aligned} \tag{18}$$

The aggregate load can now be expressed as the summation of loads at the ON-state, multiplied by the net power that every load consumes:

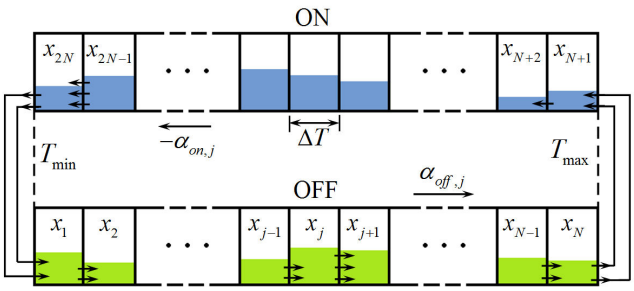

Fig. 5. Finite-difference discretization of the system for achieving load propagation dynamics between the minimum and maximum temperature limits.

$$P_T(t) = \frac{P}{\eta} \sum_{j=N+1}^{2N} x_j \tag{19}$$

Equations (17), (18) and (19) can be lumped together to form a bilinear state-space matrix representation of the system as follows:

$$\begin{aligned} \dot{x}(t) &= \mathbf{A}x(t) + \mathbf{B}x(t)u(t), \quad u(t) = \dot{T}_{sp}(t) = \lambda \dot{f}(t) \\ y(t) &= Cx(t) \end{aligned} \tag{20}$$

where $x(t) = [x_1(t), x_2(t), \ldots, x_{2N}(t)]^T$ is the $2N\times1$ state vector, $y(t) = P_T(t)$ is the aggregate power, $C = [0, \ldots, 0|_N, P/\eta, \ldots, P/\eta]$ is the $1\times2N$ state-to-output vector, $\mathbf{A}$ is the state matrix structured as:

$$\mathbf{A} = \begin{bmatrix} \frac{-\bar{\alpha}_{off}}{\Delta T} & & & & \mathbf{0} & & & & \frac{-\bar{\alpha}_{on}}{\Delta T} \\ \frac{\bar{\alpha}_{off}}{\Delta T} & \frac{-\bar{\alpha}_{off}}{\Delta T} & & & & & & & \\ & \ddots & \ddots & & & & \ddots & & \\ & & \frac{\bar{\alpha}_{off}}{\Delta T} & \frac{-\bar{\alpha}_{off}}{\Delta T} & & & & & \\ \mathbf{0} & & & \frac{\bar{\alpha}_{off}}{\Delta T} & \frac{\bar{\alpha}_{on}}{\Delta T} & & & & \mathbf{0} \\ & & & & \frac{-\bar{\alpha}_{on}}{\Delta T} & \frac{\bar{\alpha}_{on}}{\Delta T} & & & \\ & & \ddots & & & \ddots & \ddots & & \\ & & & & & & \frac{-\bar{\alpha}_{on}}{\Delta T} & \frac{\bar{\alpha}_{on}}{\Delta T} & \\ 0 & & & & \mathbf{0} & & & \frac{-\bar{\alpha}_{on}}{\Delta T} & \frac{\bar{\alpha}_{on}}{\Delta T} \end{bmatrix} \tag{21}$$

and $\mathbf{B}$ is the input matrix given by:

$$\mathbf{B} = \begin{bmatrix} \frac{1}{\Delta T} & & & & \mathbf{0} & & & & \frac{1}{\Delta T} \\ \frac{-1}{\Delta T} & \frac{1}{\Delta T} & & & & & & & \\ & \ddots & \ddots & & & & \ddots & & \\ & & \frac{-1}{\Delta T} & \frac{1}{\Delta T} & & & & & \\ \mathbf{0} & & & \frac{-1}{\Delta T} & \frac{-1}{\Delta T} & & & & \mathbf{0} \\ & & & & \frac{1}{\Delta T} & \frac{-1}{\Delta T} & & & \\ & & \ddots & & & \ddots & \ddots & & \\ & & & & & & \frac{1}{\Delta T} & \frac{-1}{\Delta T} & \\ 0 & & & & \mathbf{0} & & & \frac{1}{\Delta T} & \frac{-1}{\Delta T} \end{bmatrix} \tag{22}$$

This completes the state-space model derivation. In the next section, we further analyze and simulate the model, and compare it with the primary model for validation.

IV. Model Analysis and Simulations

In this section, we provide an eigenvalues analysis for the developed state-space model. Furthermore, we simulate the free and the forced state-space models and compare them with the primary Monte Carlo model simulations.

A. System Analysis

To examine the stability properties of the system, we start with analyzing the eigenvalues of the state matrix. Since the system is bilinear, we focus our attention on the case where the control input is zero, and stability is therefore governed by the $\mathbf{A}$ matrix only. For a constant ambient temperature, the matrix $\mathbf{A}$ does not change, and the system represents a free linear time-invariant (LTI) system. The eigenvalues of $\mathbf{A}$ can be obtained through the following characteristics equation:

$$\left[\left(\frac{N\bar{\alpha}_{off}}{\Delta_{db}} + \lambda\right)\left(\frac{N\bar{\alpha}_{on}}{\Delta_{db}} - \lambda\right)\right]^N - \left[\left(\frac{N\bar{\alpha}_{off}}{\Delta_{db}}\right)\left(\frac{N\bar{\alpha}_{on}}{\Delta_{db}}\right)\right]^N = 0 \tag{22}$$

which immediately implies that $\lambda = 0$ and $\lambda = N(\bar{\alpha}_{on} - \bar{\alpha}_{off})/\Delta_{db}$ are two real eigenvalues of the system with the latter having a negative sign.

Figure 6 shows eigenvalues of the system for different discretizations, for the parameter values listed in Table 1. As seen, the eigenvalues of the system form an ellipse on the left-half complex plane. The larger the number of finite-difference discretizations, the larger the ellipse.

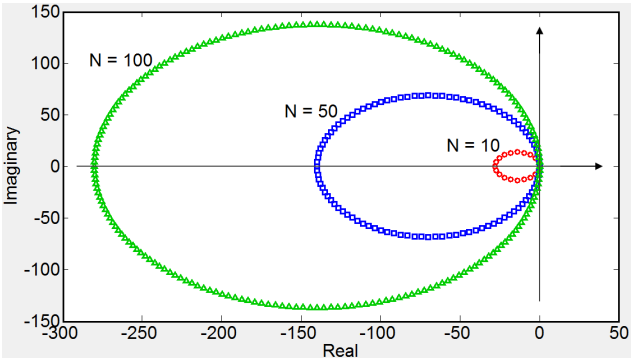

Fig. 6. Eigenvalues of the system state matrix for different discretizations.

B. Numerical Simulations

The obtained bilinear system model is numerically validated here against the primary system model. Figure 7 depicts the response of the free state-space model compared to the primary model with homogeneous parameters for the initial condition explained in section 2.2. Moreover, Figure 8 shows the comparison of the forced state-space system with the primary model under set-point temperature variation. We can see in both free and forced model simulations that the state-space model is able to accurately reproduce the response of the primary model for larger discretization numbers. In other words, the higher the resolution of the discretization, the higher the accuracy of the state-space model.

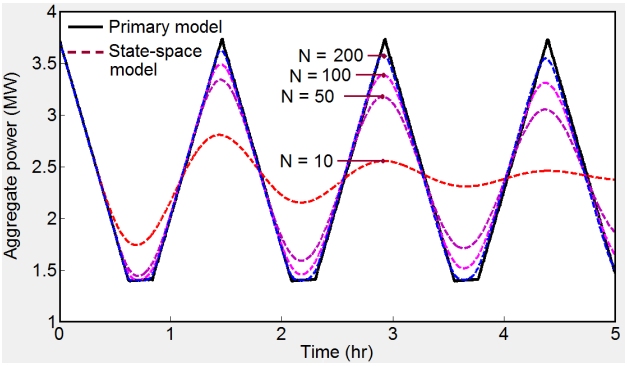

Fig. 7. Comparison between the free responses of the discretized state-space model and the primary model.

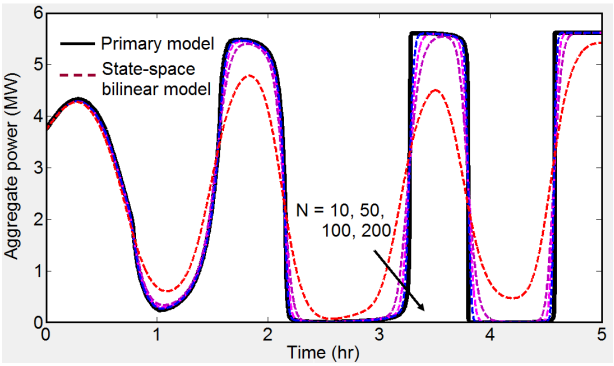

Fig. 8. Comparison between the forced responses of the discretized state-space model and the primary model (for the input shown in Fig 2).

Now that a control-oriented state-space model is developed for the aggregate TCLs, in the next section we analyze this model for the purpose of control design.

V. Control Analysis and Design for Aggregated TCLs

In this section, we use the Lyapunov theory to analyze the output controllability of the derived bilinear state-space model, and develop an asymptotically-stable control paradigm for the system. Due to the bilinearity of the system, standard controllability tests used for linear systems analysis cannot be directly employed. Thus, we use the Lyapunov method in this paper to gain useful insights into the system's output controllability.

A. Analysis of system's output controllability

To examine the system's output controllability, we start with defining a control error for the closed-loop system, and try to obtain control laws under which the control error converges to the origin, or to a small bounded region. Define the control error as:

$$e(t) = y_d(t) - y(t) \tag{23}$$

where $y_d(t)$ is the desired aggregate load trajectory to be followed by the TCLs. Next we define a positive-definite Lyapunov candidate function:

$$V(t) = \frac{1}{2}e^2(t) \tag{24}$$

The derivative of this Lyapunov function for the system described by Eq. (20) is obtained as:

$$\begin{aligned}\dot{V}(t) &= e(t)\dot{e}(t) = e(t)\{\dot{y}_d(t) - C\dot{x}(t)\} \\ &= e(t)\{\dot{y}_d(t) - C\mathbf{A}x(t) - C\mathbf{B}x(t)u(t)\}\end{aligned} \tag{25}$$

It is important to note that the term $C\mathbf{B}x(t)$ in Eq. (25) is the coefficient of the control input, $u(t)$. Therefore it plays a key role in determining the output controllability of the system. Hence, we first focus on this term, which can be simplified to:

$$\begin{aligned}C\mathbf{B}x(t) &= [0, \dots, 0, -\frac{P}{\eta\Delta T}|_N, 0, \dots, 0, -\frac{P}{\eta\Delta T}]x(t) \\ &= -\frac{P}{\eta\Delta T}\left(x_N(t) + x_{2N}(t)\right)\end{aligned} \tag{26}$$

Equation (26) indicates that in order for the control input to remain effective, the collective number of loads at the boundary segments, i.e., $x_N(t) + x_{2N}(t)$, must be nonzero for all time. This will be the necessary and sufficient condition for the system's output controllability. We will see that if this condition holds, we can design asymptotically stable feedback controllers, in the Lyapunov sense, for the output tracking control of the system.

One way to achieve the controllability condition described above is to start from a strictly nonzero initial distribution, and keep the set-point temperature variation slower than the load diffusion dynamics. This way, the continuity of the load distribution will be preserved throughout the process. Therefore, the boundary segments will always contain a number of loads. Maintaining strictly nonzero load distribution over the temperature deadband is even more feasible in practice because of the artificial damping effect created by the inherent heterogeneity of thermostatic loads.

B. State-space control design

If the system matrices **A**, **B**, C are known, the state vector $x(t)$ is measureable or observable in real-time, the desired load trajectory $y_d(t)$ is known and is differentiable, and the output controllability condition holds, i.e. $C\mathbf{B}x(t) \neq 0$, then one control design to achieve asymptotic output tracking control of the system is given by:

$$u(t) = \frac{1}{C\mathbf{B}x(t)}\{\dot{y}_d(t) - C\mathbf{A}x(t) + k_1 e(t)\} \tag{27}$$

where k_1 is a positive control gain. Note that $e(t) = y_d(t) - Cx(t)$.

To prove the asymptotic convergence property of the above control law, we replace Eq. (27) into the derivative of the Lyapunov candidate function, Eq. (25) to obtain:

$$\dot{V}(t) = -k_1 e^2(t) \tag{28}$$

The combination of Eq. (28) and (24) yields:

$$\dot{V}(t) + 2k_1 V(t) = 0 \tag{29}$$

which results in the solutions:

$$V(t) = V(0)\exp(-2k_1 t),$$
$$e(t) = e(0)\exp(-k_1 t) \tag{30}$$

This simply indicates the exponential convergence of the tracking error to zero with the rate of k_1.

A numerical simulation is provided here to illustrate the tracking performance of the proposed control law. A multiple-frequency sinusoidal desired trajectory depicted in Figure 9(a) is applied. The controller is implemented and the system is released from the same initial condition given in Sec. 2. Results indicate the convergence of the aggregate load response to the desired trajectory (subfigure 9a) and the exponential convergence of the tracking error to zero (subfigure 9b), as expected. Moreover, the setpoint temperature remains within the specified bounds (subfigure 9c), while its rate of variation remains slower than the diffusion rates of the loads. It is remarked that the state vector $x(t)$ used in the controller is directly measured from the simulated state-space model.

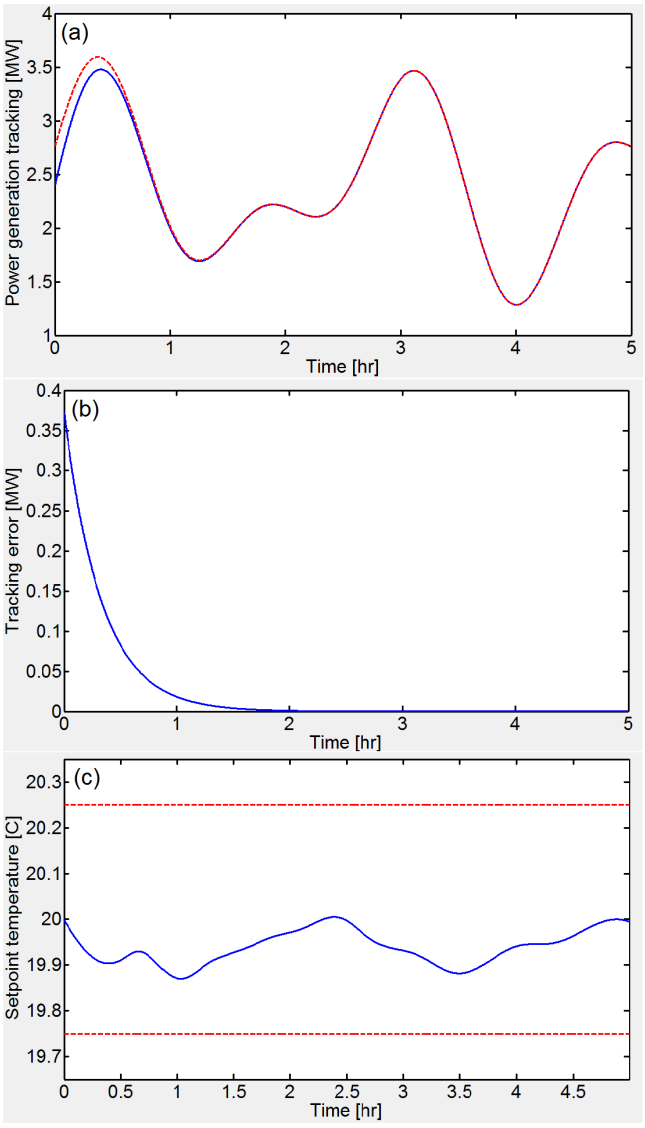

Fig 9. State-space control implementation: (a) power tracking, (b) error convergence, and (c) set-point temperature variation.

VI. Conclusions

In this paper, we developed a novel modeling and control framework for the direct load control of thermostatic air-conditioning loads using a universal setpoint temperature command. We derived the underlying partial differential equations describing the system dynamics under set-point temperature transients. The resultant model is a conditionally controllable, open-loop stable bilinear system. Using the Lyapunov stability criteria, we obtained the controllability condition, and designed a state-space feedback controller for the asymptotic output tracking control of the system. Numerical simulations were provided to show the validity of the model and the performance of the controller for load following during the demand-side load management of thermostatic air-conditioning systems.

Acknowledgment

This research was supported by a research partnership led by the University of Michigan and DTE Energy, and funded by a Michigan Public Service Commission Grant. The authors gratefully acknowledge this support.

References

[1] L. Hughes, "Meeting residential space heating demand with wind-generated electricity," *Renewable Energy*, **35**, pp. 1765-1772, 2010.

[2] D. S. Callaway, "Tapping the energy storage potential in electric loads to deliver load following and regulation, with application to wind energy," *Energy Conversion and Management*, **50**, pp. 1389-1400, 2009.

[3] S. Koch, M. Zima and G. Andersson, "Potentials and applications of coordinated groups of thermal household appliances for power system control purposes," *IEEE-PES/IAS Conference on Sustainable Alternative Energy*, September 2009, Valencia, Spain.

[4] N. Lu and S. Katipamula, "Control strategies of thermostatically controlled appliances in a competitive electricity market," *IEEE Power Engineering Society General Meeting*, **1**, pp. 202-207, San Francisco, CA, June 2005.

[5] M. W. Gustafson, J. S. Baylor, and G. Epstein, "Direct water heater load control. Estimating program effectiveness using an engineering model," *IEEE Transactions on Power Systems*, 8, pp. 137-143, 1993.

[6] T. Ericson, "Direct load control of residential water heaters," *Energy Policy*, **37**, pp. 3502-3512, 2009.

[7] D. S. Callaway and I. Hiskens, "Achieving controllability of plug-in electric vehicles," *IEEE Vehicle Power and Propulsion Conference*, pp. 1215-1220, Dearborn, MI, Sept. 2009,.

[8] M. Takagi, K. Yamaji, and H. Yamamoto, "Power system stabilization by charging power management of plug-in hybrid electric vehicles with LFC signal," *IEEE Vehicle Power and Propulsion Conference*, pp. 822-826, Dearborn, MI, Sept. 2009.

[9] W. W. Lang, M. D. Anderson, and D. R. Fannin, "Physically based modeling of cold load pickup," *IEEE Transactions on Power Apparatus and Systems*, **101**, pp. 924-932, 1982.

[10] F. D. Galiana, E. Handschin, and A. Fiechter, "Identification of stochastic electric load models from physical data," *IEEE Transactions on Automatic Control*, **19**, pp. 887-893, 1974.

[11] Y. Manichaikul and F. C. Schweppe, "Physically based industrial electric load", *IEEE Transactions on Power Apparatus and Systems*, **98**, pp. 1439-1445, 1979.

[12] R. Malhame and C. Y. Chong, "Electric load model synthesis by diffusion approximation of a high-order hybrid-state stochastic system," *IEEE Transactions on Automatic Control*, **30**, pp. 854-860.